UC Irvine
UC Irvine Previously Published Works

Title

Titrating chimeric antigen receptors on CAR T cells enabled by a microfluidic-based dosage-controlled intracellular mRNA delivery platform

Permalink

https://escholarship.org/uc/item/84x0k93s

Journal

Biomicrofluidics, 18(6)

ISSN

1932-1058

Authors

Chen, Yu-Hsi

Mirza, Mahnoor

Jiang, Ruoyu

et al.

Publication Date

2024-12-01

DOI

10.1063/5.0231595

Titrating chimeric antigen receptors on CAR T cells enabled by a microfluidic-based dosage-controlled intracellular mRNA delivery platform 🅢🅕✅

Yu-Hsi Chen; Mahnoor Mirza 🅘 ; Ruoyu Jiang; Abraham P. Lee ✉ 🅘

Check for updates

View Online   Export Citation

Articles You May Be Interested In

Electroporation mechanism decreases life-threatening side effects of cancer treatment

Scilight (December 2024)

Main issues and current strategies in enhancing the efficacy of chimeric antigen receptor T-cell therapy among tumor treatments

AIP Conf. Proc. (February 2020)

CAR T cell infiltration and cytotoxic killing within the core of 3D breast cancer spheroids under the control of antigen sensing in microwell arrays

APL Bioeng. (July 2024)

AIP Publishing

Biomicrofluidics

Special Topics Open for Submissions

Learn More

AIP Publishing

Titrating chimeric antigen receptors on CAR T cells enabled by a microfluidic-based dosage-controlled intracellular mRNA delivery platform SCI F

View Online   Export Citation   CrossMark

Yu-Hsi Chen,[1] Mahnoor Mirza,[1] (ID) Ruoyu Jiang,[1] and Abraham P. Lee[1,2,a)] (ID)

AFFILIATIONS

[1]Department of Biomedical Engineering, University of California, Irvine, California 92697, USA
[2]Department of Mechanical and Aerospace Engineering, University of California, Irvine, California 92697, USA

Note: This paper is part of the special collection, Selected Papers from IEEE-NANOMED 2023.
[a)]Author to whom correspondence should be addressed: aplee@uci.edu

ABSTRACT

Chimeric antigen receptor (CAR) T-cell therapy shows unprecedented efficacy for cancer treatment, particularly in treating patients with various blood cancers, most notably B-cell acute lymphoblastic leukemia. In recent years, CAR T-cell therapies have been investigated for treating other hematologic malignancies and solid tumors. Despite the remarkable success of CAR T-cell therapy, cytokine release syndrome (CRS) is an unexpected side effect that is potentially life-threatening. Our aim is to reduce pro-inflammatory cytokine release associated with CRS by controlling CAR surface density on CAR T cells. We show that CAR expression density can be titrated on the surface of primary T cells using an acoustic-electric microfluidic platform. The platform performs dosage-controlled delivery by uniformly mixing and shearing cells, delivering approximately the same amount of CAR gene coding mRNA into each T cell.

19 December 2024 20:54:40

I. INTRODUCTION

Chimeric antigen receptor (CAR) T-cell therapy represents a revolutionary paradigm for cancer immunotherapy and has significantly changed the landscape of cancer treatments. Moreover, CAR T-cell therapy has been used to effectively treat patients with relapsed and refractory B-cell acute lymphoblastic leukemia (B-ALL)[1,2] featuring three CD19-specific CAR agents (KYMRIAH, YESCARTA, and TECARTUS) approved by the Food and Drug Administration (FDA).[3–5] Other FDA-approved products, such as ABECMA-targeted BCMA antigen, have been used to treat multiple myeloma.[6] Despite these achievements, CAR T cells can potentially induce life-threatening toxicities, including cytokine release syndrome (CRS), neurologic toxicity, and anaphylaxis.[7] CRS is one of the most common and notorious side effects of CAR T-cell therapy, followed by the infusion of CAR T cells, which triggers systemic immune activation and causes excessive inflammatory cytokine release. Recent studies have shown that the heterogeneity of CAR expression levels in cell populations potentially determines the efficacy and safety of therapy. For instance, one study has

demonstrated the influence of CAR surface density on the safety of CAR T-cell therapy; the CAR surface density can be manipulated and controlled by increasing the transduction rate with the MND promoter (myeloproliferative sarcoma virus enhancer, negative control region deleted, dl587rev primer-binding site substituted).[8] Compared to the EF1α lentiviral promoter, the MND promoter has a higher packaging efficiency, but the reduced surface density of CAR molecules leads to a reduced cytokine release; therefore, it has a lower chance of triggering CRS. Moreover, another study comprehensively researched the impact of CAR density on CAR T-cell functionality and the clinical treatment outcome.[9] Phenotypic, functional, transcriptomic, and epigenomic analyses were performed to compare the high and low expressions of the CAR molecule (CAR[High] Cell and CAR[Low] Cell), and they concluded that CAR[High] T cells are associated with tonic signaling and exhausted phenotypes. Hence, a precisely controlled method that can manufacture CAR T cells efficiently and titrate the CAR expression density within an optimal range is desirable.

Due to their high transduction efficiency, the most common method for manufacturing CAR T cells in a clinical setting

employs viral vectors, including retroviruses and lentiviruses.[10] However, viral vectors have severe safety concerns, such as insertional oncogenesis,[11] transgene integration, and immunogenicity.[12] Moreover, heterogeneity of CAR T-cell surface-gene expression caused by various virus copies may mitigate therapeutic efficacy or even increase the toxicity of CAR T cells.[13] Bulk electroporation is another technique for delivering plasmid-based transgene systems, such as transposon/transposase systems, to introduce CAR genes into primary T cells.[14] However, high voltages, ranging from tens to a few hundred volts, are required to permeabilize cell membranes and potentially cause cell mortality,[15] a significant limitation in applying electroporation in clinical trials.[16] Furthermore, several studies have shown that bulk electroporation perturbs the function of cells. DiTommaso *et al.* comprehensively characterized electroporation-induced disruption of gene expression, cytokine production, and compromised *in vivo* biological functions.[17] In addition, owing to its lack of mixing between cells and genetic materials, bulk electroporation does not offer uniform and dosage-controlled delivery across cell populations.[18]

Miniaturized microfluidic intracellular delivery systems have emerged as a potential solution to overcome the limitations of low cell viability from conventional electroporation. For instance, microscale electrodes have been integrated into microfluidic platforms to achieve cell membrane permeabilization.[19] The continuous-flow microfluidic electroporation platform proposed by Lissandrello *et al.* can achieve a high green fluorescent protein (GFP)-messenger ribonucleic acid (mRNA) transfection efficiency into primary T cells without compromising cell viability by precisely controlling the electric field exposure experienced by the cells. Another example is using a microfluidic platform to apply mechanical forces to manipulate cell membranes. Jarrell *et al.* demonstrated the implementation of vortex shedding in a microfluidic platform to facilitate intracellular mRNA delivery into primary human cells.[20] However, these miniaturized transfection platforms cannot control the dosage of the delivered cargo or have low throughput. In contrast, certain mechanoporation methods can control dosage,[21–23] but they are prone to clogging and low throughput issues and have yet to prove uniform delivery.[24]

In a previous study, we developed an intracellular delivery microfluidic system, the acoustic-electric shear orbiting poration (AESOP) platform, which can disrupt the cell membrane by using the lateral cavity acoustic transducer (LCAT) technology to apply localized mechanical shear to cells via oscillating air–liquid interfaces and expanding these shear-induced nanopores through a low-intensity electric field.[25] We demonstrated high throughput (10^6 cells per minute for each chip) and enabled the uniform delivery of large cargo without compromising cell viability. In this study, we explore the application of CAR T-cell manufacturing and the manipulation of CAR expression levels on primary T-cell membranes to achieve dosage control via uniform mixing and uniform shearing.[25] With the assistance of microstreaming vortices induced by acoustic energy, CAR mRNA is mixed uniformly with primary T cells; thus, each cell uptakes approximately the same dosage of mRNA, which leads to a similar CAR expression on the cell membrane in the cell population after mRNA translation. We utilize mRNA to transiently reprogram T cells to express CAR, and since mRNA does not integrate DNA into the host genome,[26] it avoids

potential risks associated with genetic integration and circumvents on-target off-tumor toxicity caused by permanent CAR expression.[27,28] The transient expression of CAR mRNA limits the long-term therapeutic effect of mRNA-based CAR T-cell systems, making it less suitable for cases where long-term CAR expression is needed for complete response (solid tumors, aggressive cancers) or repeated dosage causes anaphylactic shock.[29] While clinical trials employing mRNA-based CAR T-cells targeting CD123 and CD19 in solid tumors targeting mesothelin and c-Met proved safe and lacking in serious adverse events, repeated dosing was required.[30] Besides repeated dosage, CAR mRNA persistence can be improved by modifying mRNA to provide a cap structure and poly(A) tail, replacing unstable non-coding sequences with stable sequences (β-globin) and codon optimization.[31] Despite limitations, mRNA-transfected CAR T cells allow for temporal control, dose adjustment, enhanced safety, and precision targeting,[32] serving as the ideal system for the study of dosage-controlled delivery explored in this paper. Additionally, though plasmid is also a common vector for carrying the CAR gene and delivering it into T cells because of simpler and cheaper manufacturing, mRNA size is smaller than plasmids, making it easier to perform primary T-cell transfection.[33] We show that the dosage taken by the cells and CAR expression levels can be titrated by controlling the initial input mRNA concentration. Moreover, the gene expression profile and cytokine secretion function did not change after AESOP treatment. These results reveal that AESOP's delivery mechanism can maintain cell therapy's safety and function and improve CAR T-cell products' homogeneity, which is a critical factor in determining the outcome of a clinical treatment.

II. RESULTS

The schematic of isolating primary T cells and transfecting T cells with AESOP and electroporation, respectively, is presented in Fig. 1. AESOP first relies on the lateral cavity acoustic transducer (LCAT) technology to trap cells inside acoustic microstreaming vortices and expose them to uniform mechanical shear. Trapped microbubbles oscillating in lateral slanted dead-end side channels generate a first-order oscillatory flow at the air–liquid interface. The first-order oscillatory flow induces a second-order streaming flow consisting of an open microstreaming flow and a closed-loop microstreaming vortex. The open microstreaming generates bulk flow that pumps through the main channel. The LCAT is powered by a piezoelectric transducer (PZT) attached to the bottom of the device, and the acoustic energy from the PZT is transmitted to the air–liquid interfaces, causing them to oscillate and generate microstreaming vortices in the microfluidic channel. The orientation and positioning of the air–liquid cavities resulted in both bulk-flow liquid pumping and size-dependent trapping of cells. The trapped cells orbiting in these microvortices were subjected to oscillatory mechanical shear stress, with the maximum shear adjacent to the oscillating air–liquid interfaces.

A. Characterization of the shear force within acoustic microstreaming vortices

We previously used LCATs with 112 pairs of dead-end side channels combined with a single main channel to perform
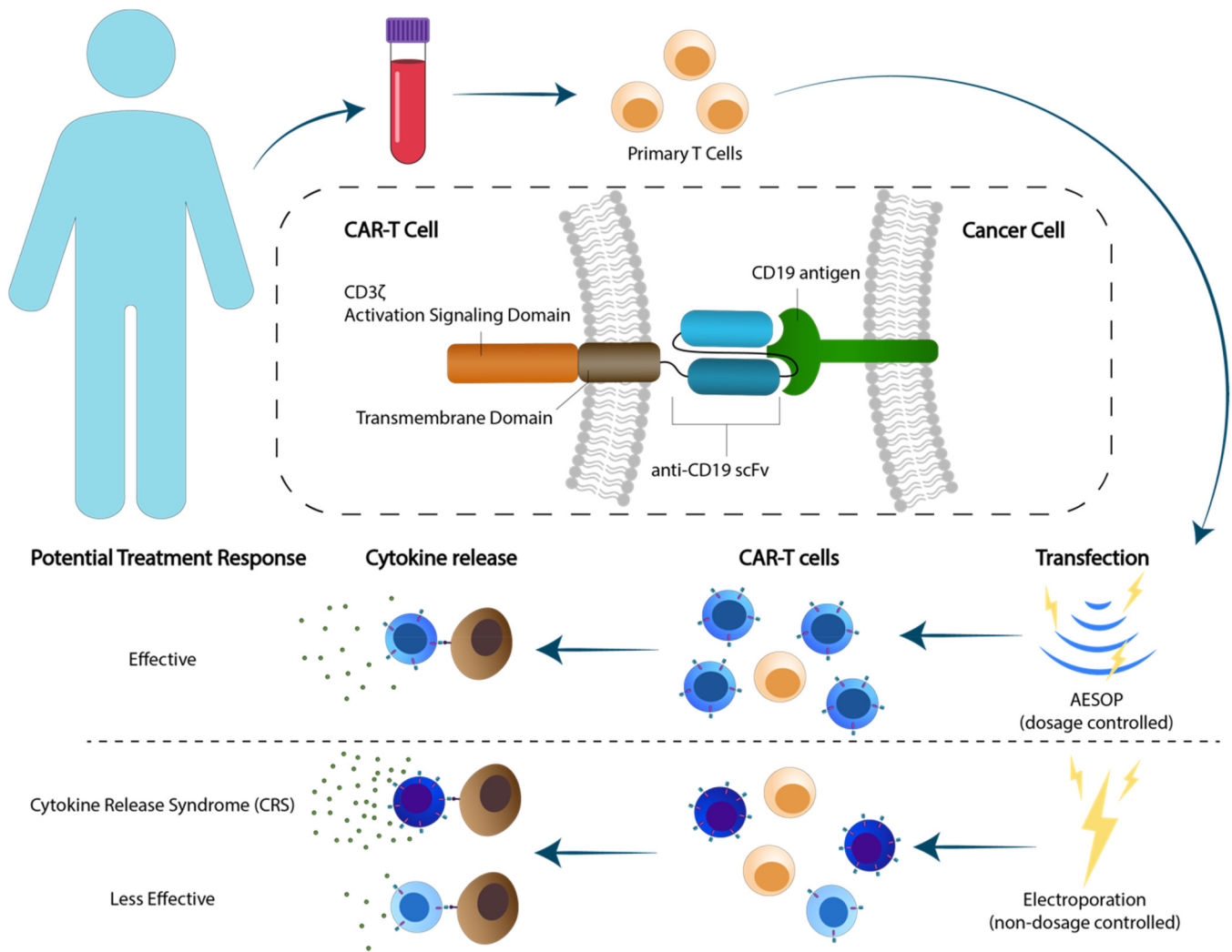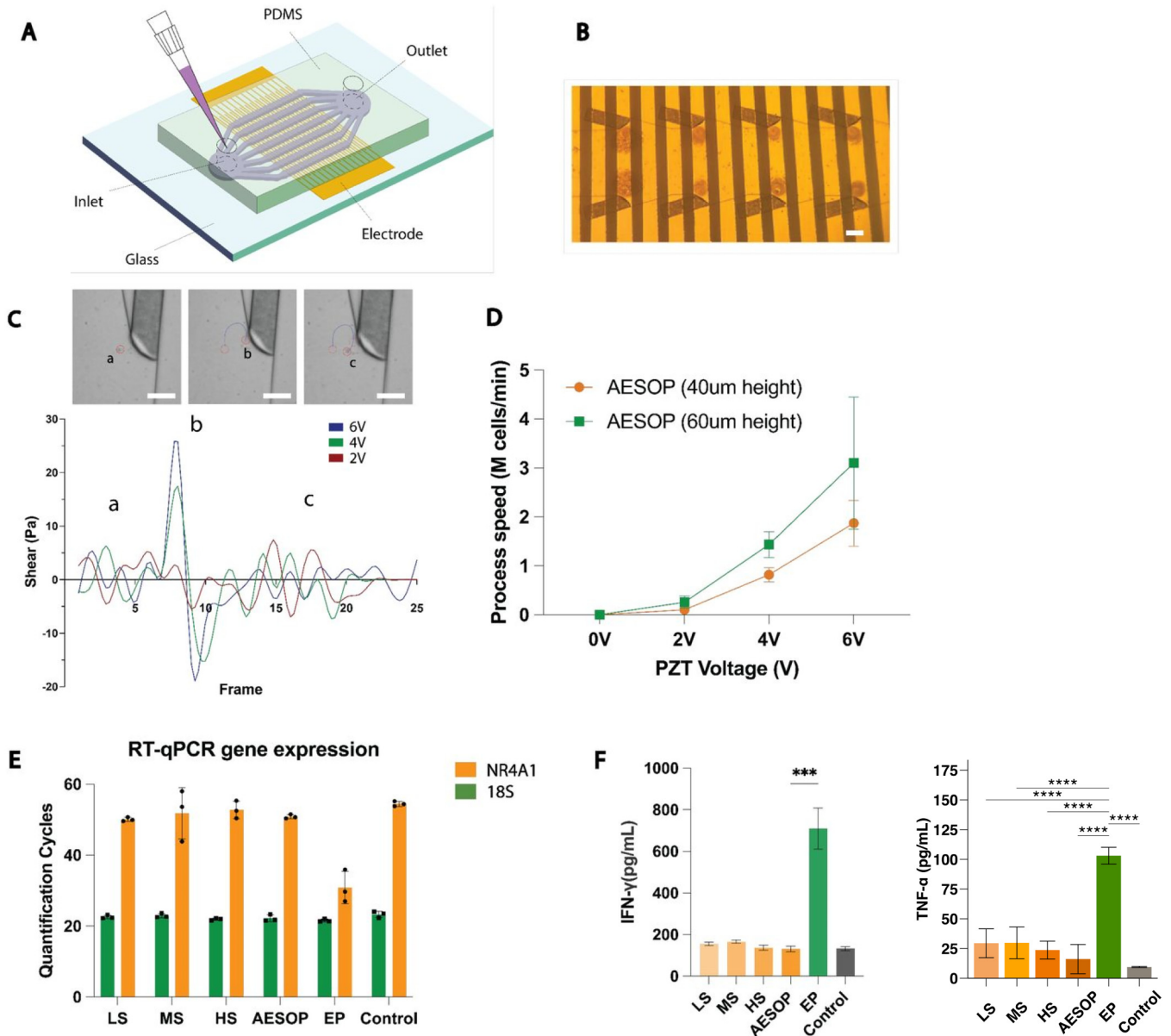
FIG. 1. Schematic of CAR T-cell generation from the isolation of primary T cells from healthy donors, T-cell activation, and transfection with AESOP and electroporation. High, medium, and low CAR-expression levels on the T-cell membrane cause CRS and potentially effective and less effective treatment responses, respectively.

self-pumping, cell-cargo mixing, and cell-membrane permeabilization. We demonstrated a throughput of 10^6 cells per minute for each chip with high delivery efficiency (>90%), cell viability (>80%), and uniform dosages [<60% coefficient of variation (CV)]. In clinics, around 0.2×10^6 to 5.4×10^6 transduced T cells per kilogram of body weight are required for anti-CD19 CAR T-cell therapy.[34] In the current study, we modified the previous serial channel design into seven parallel microfluidic channels with the same number of LCAT pairs [Figs. 2(a) and 2(b)]. Previously, to ensure maximum throughput, we introduced the electric field to the cells when almost all LCATs (vortices) in the chip were filled. With parallel channels, the cells can fill multiple vortices simultaneously, reducing the operation time and allowing more even exposure to shear as each cell remains in a vortex for similar amounts of

time. As a result of the even shearing, the CV% is further reduced compared to the serial channel device for >10^6 cells/min, and uniform delivery to T cells is improved. To characterize the device, we measured the cell traveling velocity within the acoustic microstreaming and derived the shear force that cells experienced (supplementary material, Note). More specifically, cells exhibited a faster velocity near the air–liquid interface compared to the velocity of the cells when they were away from the air–liquid interface. As a result, the acoustically activated microbubble generates microstreaming and exerts mechanical shear that deforms the cells orbiting in these microvortices. In Fig. 2(c), the cells experienced the highest amount of shear (~25 Pa) at location "b" near the air–liquid interface. When the cells moved away from the air–liquid interface, they experienced lower shear force. As the applied voltage

FIG. 2. Characterization of AESOP. (a) Schematic diagram of the parallel AESOP platform. (b) Microscopic image of cells trapped in acoustic microstreaming vortices. The scale bar is 100 μm. (c) Cells experience shear measurements in vortices under PZT operation voltages of 2, 4, and 6 V over time. The scale bar is 100 μm. (d) The parallel AESOP platform's process speed and throughput (million cells/min) under PZT operation voltages of 2, 4, and 6 V PZT with 40 and 60 μm channel heights. (e) Quantified human 18S and NR4A1 mRNA expression levels in T cells after electroporation and AESOP processing, which include low shear (2 V PZT voltage), moderate shear (4 V PZT voltage), and high shear (6 V PZT voltage) and AESOP (moderate shear and electric-pulse triggered). (f) T-cell IFN-γ and TNF-α measurement by ELISA after electroporation and AESOP processing (n = 2, donors = 2).

increased from 2 to 6 V, the microbubble oscillation increased and, in turn, increased the microstreaming velocity. The shear stress cells experienced at location "b" increased from 5 to 25 Pa. Here, we further explored the relationship between the microfluidic channel height and throughput within the AESOP device; as the height increased from 40 to 60 μm, the number of processed cells also increased [Fig. 2(d)]. At the 6 V_{PP} condition, throughput increased from 1.8 M at a height of 40 μm to 3.2 M per minute at a height of 60 μm, therefore, all experiments moving forward utilized the 60 μm height device. Furthermore, we evaluated the safety of the AESOP

transfection process by determining if any genotype and phenotype disruption occurred in the primary T cells. Thus, the NR4A1 gene expression level, a critical regulator to induce T-cell dysfunction,[34] is measured through RT-qPCR to quantify gene regulation after transfection. For comparison, different levels of shear, ranging from low shear (LS) to moderate shear (MS) and high shear (HS), as well as AESOP and electroporation (EP), were applied to transfect the primary T cells. No transfection process was performed in the control group. Human 18S gene, a housekeeping gene, was used as a control gene for the RT-qPCR experiment [Fig. 2(e)]. The results showed that the NR4A1 expression level increased only in the electroporation group and was preserved in the LS, MS, HS, AESOP, and control groups. T-cell function was also assessed by measuring cytokine release via ELISA [Fig. 2(f)]. We observed a significant disruption in cytokine secretion after the electroporation process, with substantial increases in pro-inflammatory cytokines, IFN-γ, and TNF-α, compared to the control group, all shear groups, and AESOP. This outcome indicates CAR T-cells engineered using the electroporation process has elevated potential to cause CRS in patients. The RT-qPCR and ELISA results confirmed that the acoustic-electric microfluidic platform we developed for intracellular delivery is safe and can preserve primary T-cells' genotype and cytokine release function.

## B. Uniform delivery is enabled by mixing in microstreaming vortices

We evaluated the performance of AESOP in intracellular delivery and transfection of mRNA. First, we mixed 500 kDa dextran, which is in a similar size range as mRNA,[35] with T-cell pellets. Then, we pipetted 20 μl of the cell solution into the chip inlet to prime the device and form an air–liquid interface. Finally, we apply the PZT voltage and electric field for the AESOP operation. After 1–2 min of cell mixing through acoustic microstreaming, we collected the T cells and seeded them in a 48-well culture plate. After 2 h, we determined delivery efficiency using flow cytometry. The delivery efficiency in the AESOP group was 76% ± 9.76%, while the electroporation group's was 47.5% ± 12.74%, as shown in Fig. 3(a). In addition, the cell viability in the AESOP group was 80.4% ± 5.48%, compared to the 44.93% ± 8.29% cell viability in the electroporation group. In preparation for flow cytometry, the transfected samples are washed in a microcentrifuge, and dead cells are often removed with the supernatant. For our electroporation group, 120– 200 000 from the input of 10^6 cells remained during flow cytometry processing, indicating that the actual transfection and cell viability rates may be lower than that stated. For AESOP, the cell counts remained essentially unchanged before and after transfection. We subsequently delivered eGFP mRNA (0.05 mg/ml) into primary T cells and measured the transfection efficiency for the GFP protein expression 24 h after the mRNA was delivered. The results showed that AESOP achieved >70% transfection efficiency, with >70% viable cells. In contrast, electroporation groups showed a transfection efficiency and cell viability of approximately 50%.

In the AESOP platform, acoustic microstreaming vortices played a crucial role in uniformly mixing cells and cargoes and delivering a similar amount of cargo into each cell. We used 500 kDa dextran to quantify the uniformity of cellular uptake across the cell population. The percentage coefficient of variation (%CV, which is calculated as the percentage of the standard deviation to the mean) of the fluorescence intensity across the cell population was calculated to quantify uniformity. The lower the value of %CV, the more monodisperse the fluorescence intensity across the cell population, which indicates a more uniform dextran dosage taken by the cells. Conversely, the higher the value of %CV, the more varied the dextran dosage the cells take. A cell-sized double emulsion (DE) encapsulating dextran solution in the inner phase was used as a positive control group, mimicking the situation where the cell uptake is uniform. Compared to the electroporation (EP) group, in which %CV was 97%, the %CV of the AESOP group was approximately 53.6% and was closer to that of the DE group, with a %CV of 52.5% [Fig. 3(c)]. Single-cell and DE images were acquired using a flow cytometer [Fig. 3(d) and S1 in the supplementary material]: DE and AESOP cell images showed uniform fluorescence intensities within each group, whereas cell images from the electroporation group appeared to be nonuniform, with visible differences in terms of the fluorescence intensity. According to the results, AESOP performed intracellular delivery more uniformly than electroporation by reducing %CV from 97% to 53.6%. To evaluate whether %CV is an accurate measure of uniform delivery, we used an antibody-binding capacity bead assay to establish the number of eGFP molecules in our transfected cells. In AESOP-transfected cells, there was less variation in the number of eGFP molecules compared to electroporation-transfected cells [Fig. 3(e)]. Additionally, the median AESOP-transfected cell was less saturated, with ~31 000 molecules, compared to electroporation-transfected cells containing ~74 000 molecules [Fig. 3(f)]. Taking these results with the %CV values, we can conclude that AESOP delivers cargo into cells with greater uniformity.

C. Dosage-controlled capability and mechanism of intracellular delivery

The LCAT technology utilizes the principle of acoustic microstreaming by trapping air bubbles in liquid for micromixing induction.[36] Previous studies proved that micromixing is imperative for dosage-controlled delivery as AESOP generated the narrowest distribution of plasmid DNA delivery compared to two groups without LCAT and maintained uniform delivery while increasing the mean fluorescent intensity (MFI) of transfected cells.[25] In Sec. II B, we showed that the modified AESOP platform could deliver dextran into the cell population uniformly with fluid mixing induced by acoustic microvortices. Therefore, we hypothesized that by adjusting the input concentration of reagents, the dosage required by each cell can be controlled because uniform delivery ensures each cell uptakes an average amount of cargo. To test this hypothesis, we delivered various dextran concentrations (from 0.5 mg/ml, 1, 2, 4, and 8 mg/ml) into primary T cells using AESOP with 2 V PZT voltage, and 100 V_{pp} electric voltage, 30 kHz, and 200 cycles for electric pulses. We observed fluorescence intensity across the cell population with flow cytometry. According to the fluorescence intensity histogram, the fluorescence intensity peaks in the AESOP groups increased as the dextran concentration increased. In contrast, the fluorescence peaks in the electroporation
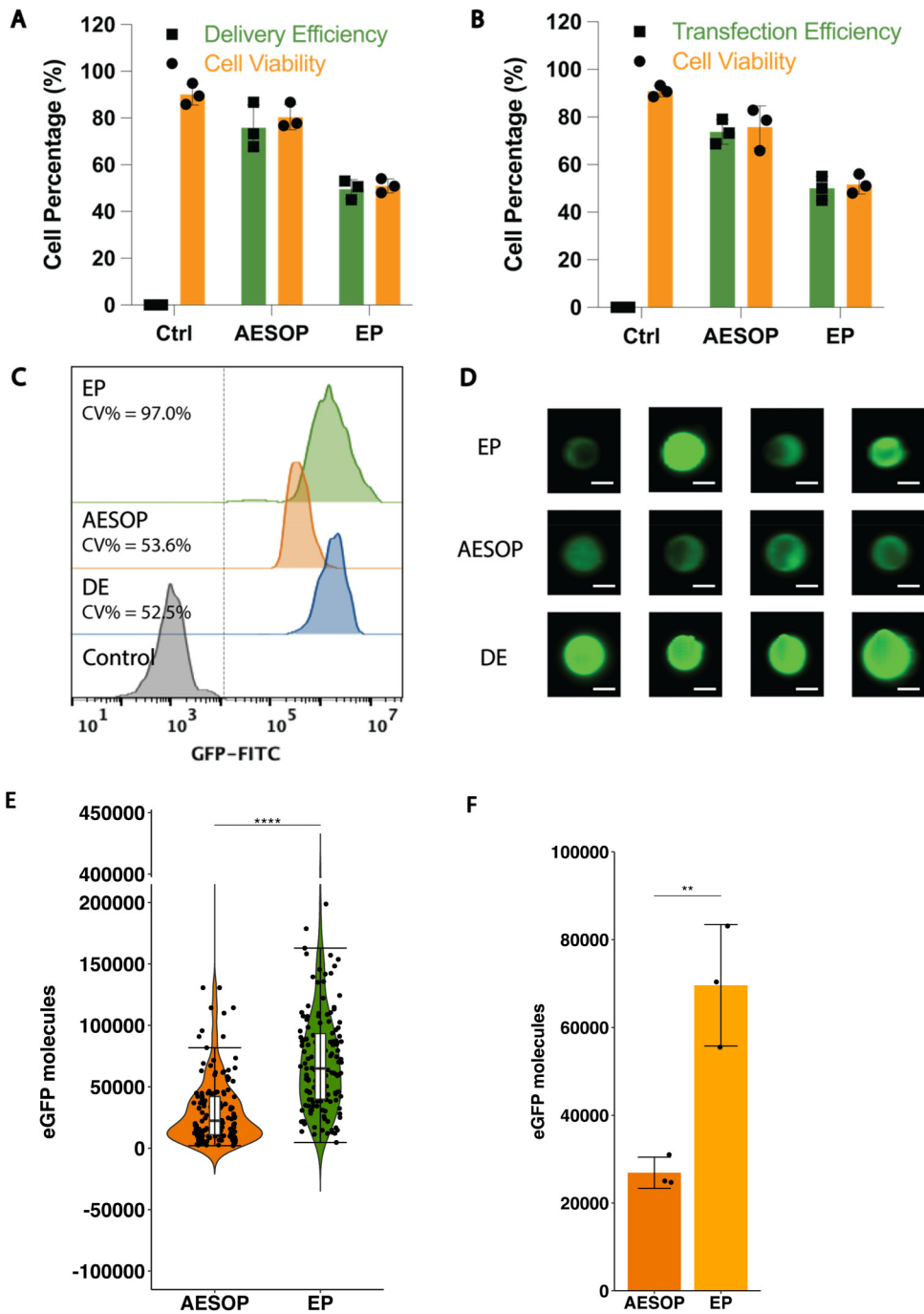
FIG. 3. Efficiency and uniformity of AESOP for delivering 500 kDa dextran and eGFP mRNA. (a) Delivery efficiency and cell viability results measured 2 h after the delivery of 500 kDa dextran. (b) Transfection efficiency and cell viability results measured 24 h after the delivery of eGFP mRNA. (c) %CV to quantify the uniformity of delivery between AESOP, electroporation, and double emulsion (DE) groups. All the histograms depict transfected cells only (except control group) and were normalized for better comparison between each group. (d) Single-cell images after delivering 500 kDa dextran among electroporation, AESOP, and double emulsion (DE) groups. The scale bar in all images is 7 μm. (e) and (f) Quantification of eGFP molecules in T cells using an antibody-binding bead assay (n = 3). Tukey's honest significant difference (HSD) test was used to test significant differences between means. (e) Single-cell values of eGFP molecules (50 cells/replicate/donor) (f) The median value of eGFP molecules/replicate/donor.

groups did not increase once the dextran concentration was higher than 1 mg/ml [Fig. 4(a)]. As illustrated in Fig. 4(b), we calculated the mean fluorescence intensity (MFI) from the flow cytometry histogram results for different dextran concentrations. Based on these results, the MFI, which quantifies the amount of dextran delivered into cells, was linearly related to the dextran concentration in the AESOP groups rather than the electroporation groups. We then applied reciprocal fitting to the MFI at various concentrations, and the R-squared values for the AESOP and electroporation groups were 0.99 and 0.83, respectively, with the former indicating a higher fitness and suggesting that AESOP enables dosage-controlled delivery capabilities.

To further investigate the performance of controlled protein expression by AESOP, which is positively correlated with mRNA abundance uptake by the cells,[37] we introduced eGFP mRNA into primary T cells and measured the GFP expression level in the cell population using a flow cytometer. The dosage of eGFP mRNA (0.5, 1.0, and 1.5 μg) was used for cell transfection. The results demonstrated that AESOP could control the expression levels of GFP protein by observing an increasing trend of fluorescence intensity as the mRNA dosage increased. The trend was evidenced by the fluorescence histogram peaks shifting to the right. Although the transfection efficiency increased for the electroporation groups, the fluorescence histogram peaks remained at approximately the same value without a dynamic shift when the mRNA dosage increased [Fig. 4(c)]. At higher concentrations of eGFP mRNA (5 and 10 μg), electroporation transfection efficiency did not change, and MFI of transfected cells varied slightly and was donor-dependent (Fig. S5 in the supplementary material).

D. CAR mRNA transfection and CAR T-cell generation with dosage control

In the previous section, we proved that AESOP could deliver and control the dosage of cargoes, thus titrating the protein expression level by eGFP mRNA as a proof of concept. In this section, CAR mRNA encoding anti-CD19 and GFP-reporter (Fig. S2 in the supplementary material) was manufactured from the pSLCAR-CD19-CD3z plasmid[33] by *in vitro* transcription (IVT), is used to test CAR mRNA transfection. To verify whether the GFP reporter is a proper indicator of the CAR gene (anti-CD19), we measured the relationship between the GFP reporter and CAR expression. Transfected cells were labeled with anti-CD19 APC [Fig. 5(c)]. Linear correlation was observed between APC and GFP fluorescence intensity, indicating that the GFP reporter was a proper indicator of CAR expression [Fig. S3 in the supplementary material]. First, we explored the performance of AESOP for the intracellular delivery of CAR mRNA and obtained the transfection efficiency according to the GFP reporter 24 h after the experiment. According to the results, the AESOP group showed 64% transfection efficiency and 80% cell viability compared to the electroporation groups, which had transfection efficiency and cell viability at approximately 35% [Figs. 5(a) and 5(b)]. Finally, we delivered three different dosages of CAR-mRNA (2.5, 5.0, and 7.5 μg) into primary T cells to investigate the corresponding CAR expression level. Based on these results, the APC fluorescence intensity, which corresponded to the CAR expression level on the cell membrane, increased when the dosage of CAR mRNA increased in AESOP. However, the CAR expression levels were widespread in the electroporation group, and no fluorescence intensity shifts were observed as the CAR mRNA dosage increased.

III. MATERIALS AND METHODS

A. Materials and reagents

Fetal bovine serum (FBS), Iscove's modified Dulbecco's medium (IMDM), Dynabeads CD3/CD28, and recombinant human interleukin-2 (IL-2) protein (Invitrogen) were purchased from Thermo Fisher Scientific. ImmunoCult-XF T Cell Expansion Medium and immunomagnetic negative selection kits were purchased from STEMCELL Technologies. FITC-dextran molecules (500 kDa) were purchased from Millipore Sigma. CleanCap-Enhanced Green Fluorescent Protein mRNA (L-7601) was purchased from TriLink Biotechnologies. APC-Labeled Human CD19 Protein was purchased from Acro Biosystems.

B. AESOP device fabrication

AESOP integrates Interdigitated Array (IDA) electrodes with an LCAT microfluidic chip. For the IDA electrode fabrication, we used the lift-off technique. At the beginning of the lift-off process, the positive photoresist MICROPSIT S1813 was patterned with the outline of the electrode as a standard photolithography protocol. E-beam evaporation was performed to deposit 300 Å of chromium (Cr) followed by 1000 Å of gold (Au) on glass slides. Finally, the glass slides were sonicated in an acetone bath to remove the unwanted metal photoresist and the metal layer. For the microfluidic part, standard photolithography was used to fabricate the negative mold, in which a negative photoresist SU-8 2075 (Kayaku Advanced Materials, Inc.) was used for pattern fabrication on a silicon wafer. Finally, a polydimethylsiloxane (PDMS) (Sylgard 184, Dow Corning) base was mixed with a curing agent at a 10:1 ratio and poured onto the silicon wafer mold, degassed for 1 h in a vacuum chamber, and cured at 65 °C overnight. Finally, the cured PDMS was bonded onto the glass slide with the electrode after the oxygen plasma treatment and baked overnight at 65 °C to allow the PDMS device to recover its hydrophobicity.

C. Primary T-cell isolation and culture protocols

Blood samples from healthy donors were obtained from the Institute for Clinical and Translational Science (ICTS) at the University of California, Irvine. Within 12 h of blood collection, primary T cells were isolated using immunomagnetic negative selection kits (STEMCELL Technologies) according to the suggested protocols. After isolation, the T cells were mixed with PBS-washed CD3/CD28 Dynabeads at a cell-to-bead ratio of 1:1. Isolated T cells and Dynabeads were cultured in the ImmunoCult-XF T Cell Expansion Medium with 30 U ml^{-1} human IL-2 recombinant protein at 37 °C in a humidified 5% CO$_2$ incubator for 3 days at a seeding density of 1×10^6 cells ml^{-1}. Each "n" refers do a donor; n = 3 is three replicates, an experiment from each of the three donors. AESOP and bulk EP were tested with the same donors.
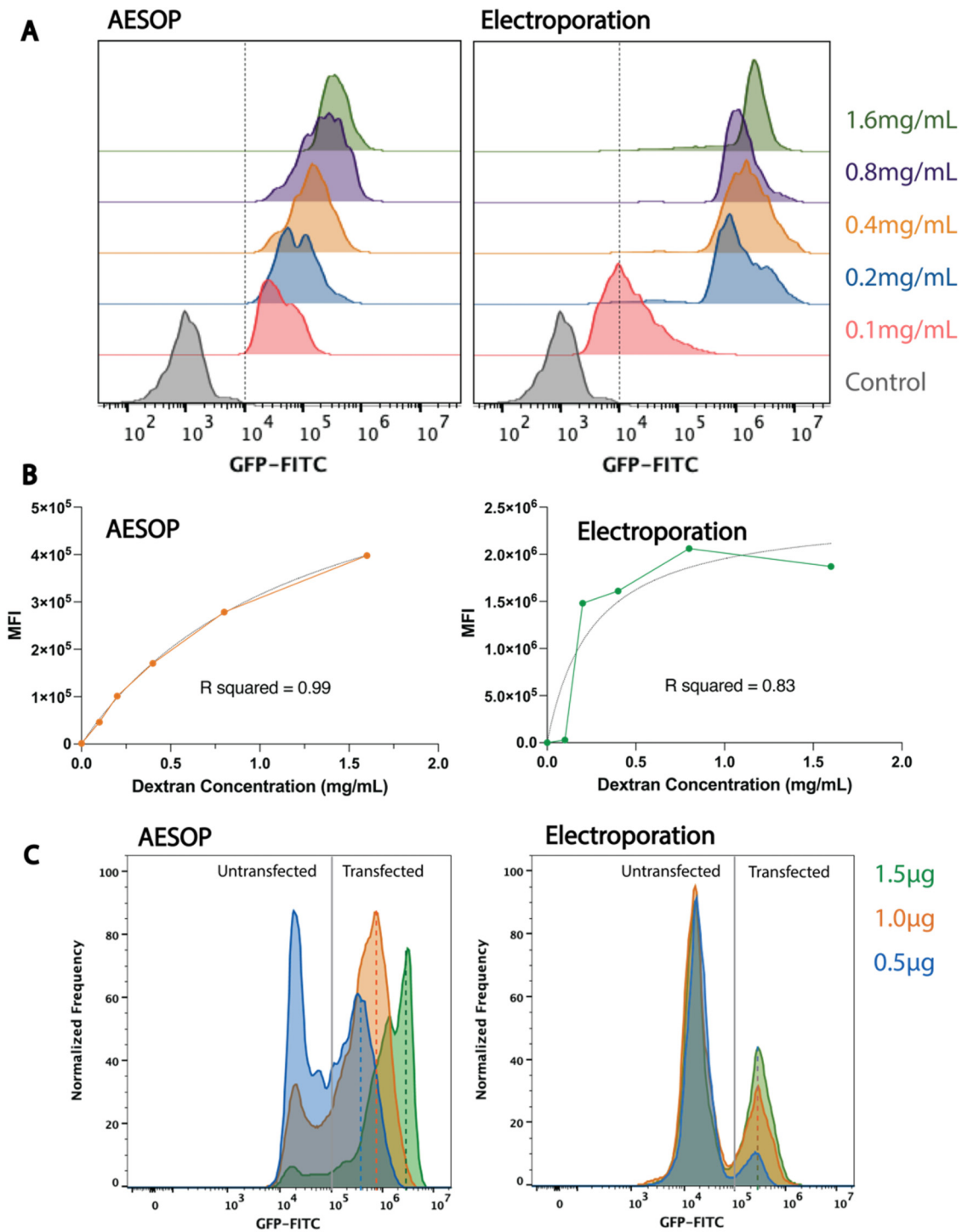
FIG. 4. Dosage-controlled delivery and protein expression-level manipulation by AESOP. (a) Flow cytometry histogram of GFP fluorescence intensity of various input dextran concentrations. (b) Line graph showing the linear correlation between the mean fluorescence intensity (MFI) and dextran concentration. The R-squared values in AESOP and electroporation groups are 0.99 and 0.83, respectively. (c) Flow cytometry histogram of the GFP protein expression under different dosages of eGFP mRNA. The dashed lines indicate the mean GFP protein expression level corresponds with various dosages of mRNA.
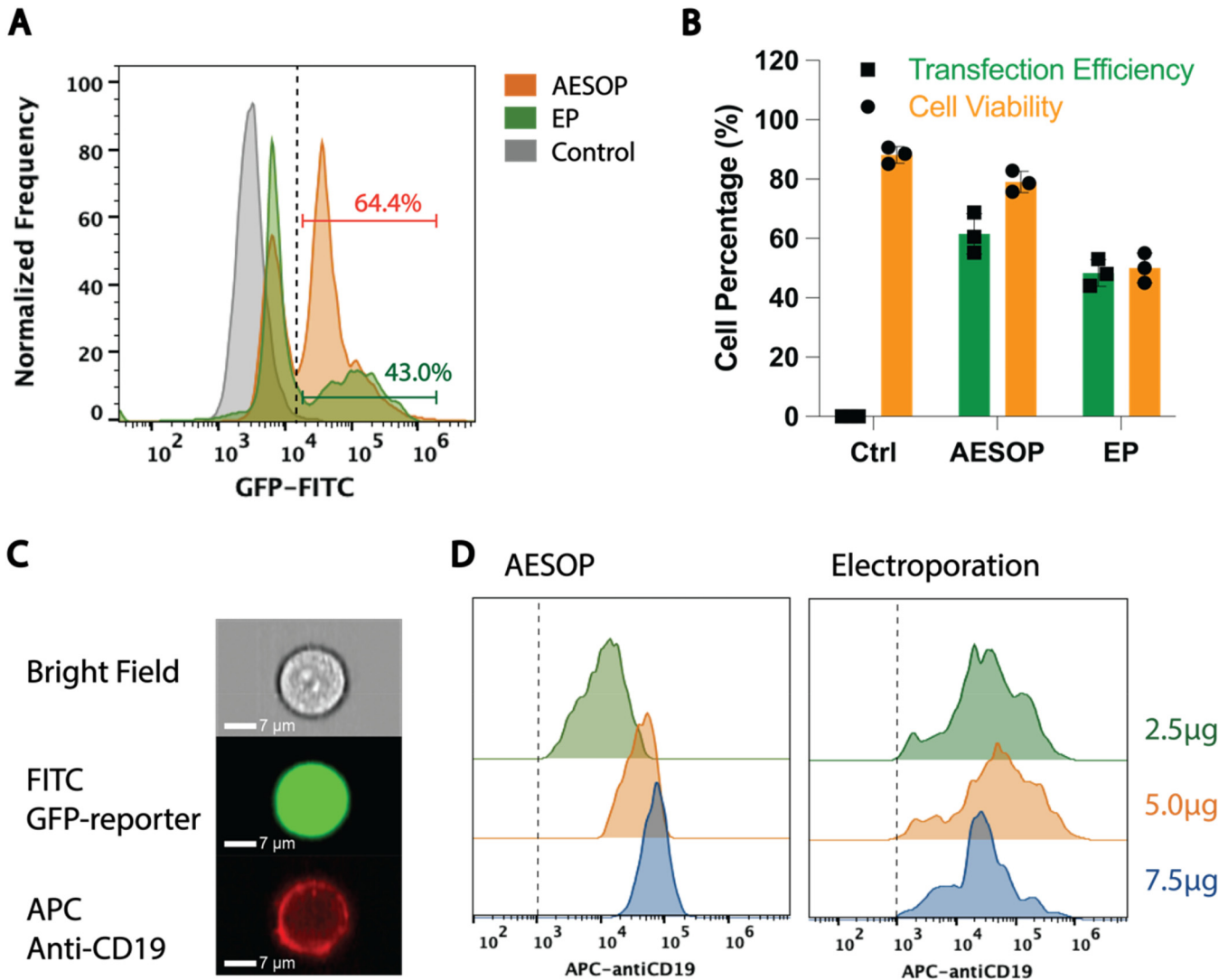
FIG. 5. AESOP performance of CAR mRNA transfection and control of the CAR expression into the T-cell population. (a) Flow cytometry histogram for quantifying CAR mRNA transfection efficiency according to GFP reporter. (b) Transfection efficiency of CAR mNRA and cell viability of T cells measured 24 h after intracellular delivery. (c) Magnified image of single CAR T cells with GFP reporter and label of anti-CD19 stained with an APC stain. (d) The histogram of fluorescence intensity used to measure anti-CD19 expression levels under various CAR mRNA dosages.

D. CAR mRNA synthesis

pSLCAR-CD19-CD3z was a gift from Scott McComb (Addgene plasmid No. 135993; http://n2t.net/addgene:135993; RRID:Addgene_135993).[33] *In vitro* transcription (IVT) was performed by TriLink Biotechnologies to synthesize mRNA encoding CAR-CD19.

E. Setup of the RT-qPCR

The genotype of human primary T cells was characterized after processing with AESOP and electroporation. RT-qPCR was performed and measured in human 18S and NR4A1 mRNA expression quantitatively 3 days after the process. The Quick-RNA Microprep Kit purchased from Zymo Research was used to lyse cells, extract RNA, and purify RNA according to the manufacturer's protocol. NanoDrop 2000 spectrometers were used to measure the concentration and purity of the RNA samples (260/280 > 2.0). Next, the iScript™ cDNA Synthesis Kit (Bio-Rad) was used to synthesize 500 ng RNA from each sample into cDNA products, and the thermocycler protocol was 25 °C for 5 min, 42 °C for 30 min, 85 °C for 5 min, and then 4 °C for 10 min. Finally, 20 μl of RT-qPCR mix was prepared with 10 μl SYBR™ Green PCR Master

Mix (Thermo Fisher Scientific), 8 μl cDNA products, and 1 μl each forward and reverse primer. A S1000 Thermal Cycler (Bio-Rad) was used with the following thermal cycling setup: 95 °C for 3 min, 95 °C for 10 s, then 55 °C for 30 s, which repeated for 40 cycles. The sequences of the forward and reverse primers for human 18S rRNA were 5′-ATTCGAACGTCTGCCCTATCAA-3′, and 5′-CGGGAGTGGGTAATTTGCG-3′, respectively. The sequences of the forward and reverse primers for NR4A1 were 5′-ATGCCTCCCCTACCAATCTTC-3′, and 5′-CACCAGTTCCTG GAACTTGGA-3′, respectively. All the primers were purchased from Integrated DNA Technologies.

F. Flow cytometry analysis

After transfection with AESOP and eGFP or CAR mRNA, T cells were incubated in ImmunoCult-XF T Cell Expansion Medium and immunomagnetic negative selection kits were purchased from STEMCELL Technologies. After 24 h, the cells were washed and resuspended in a flow cytometry buffer (2% FBS in PBS). For the cell viability assay, Calcein Red or Blue AM (AAT Bioquest) was added to the cell solution at a 1:100 volume ratio to stain live cells. According to the manufacturer's protocol, T cells were stained with APC-labeled Human CD19 protein (Acro Biosystems) for CAR T-cell transfection. The cell samples were then scanned using an ImageStream Mark II Imaging Flow Cytometer (Amnis Corporation) at 60× magnification. Cell viability, transfection efficiency, and fluorescence intensity (%CV) were analyzed using IDEAS, a simulation software (Amnis Corporation), and FlowJo. The flow cytometry gating strategy is shown in Fig. S4 in the supplementary material.

G. T cells IFN-γ and TNF-α release measured by ELISA kit

IFN-γ release by T cells was quantified using ELISA MAX™ Standard Set Human IFN-γ purchased from BioLegend. According to the manufacturer's instructions, all reagents not included in the kit were purchased from BioLegend. Standard curves and samples were prepared according to the manufacturer's instructions. A BioTek Cytation5 plate reader was used to acquire results using a colorimetric mold. TNF-α release was quantified using BD OptEIA™ Human TNF ELISA Kit II from BD Bioscience, according to the manufacturer protocol. Absorbance was read using an ELISA plate reader, Spectra Max ABS Plus (Molecular Devices).

H. Electroporation transfection experiment

All electroporation experiments were performed using the Lonza Nucleofector Transfection 4D Device. The electroporation buffer and cuvettes were obtained from the P3 Primary Cell 4D-Nucleofector™ X Kit L and prepared according to the manufacturer's protocol. The electroporation program used for stimulated primary T cells was included in the electroporator (EO-115).

I. Antibody-binding capacity bead assay

The number of eGFP molecules in T cells isolated from healthy donors was quantitated using Quantum Simply Cellular (Bangs Laboratories, USA, Catalog No. 816) according to the

manufacturer's protocol. The antibody used to perform bead conjugation was the Human IgG Fluorescein-conjugated Antibody (R&D systems, catalog No. F0158). Using calibration curves generated by running the fluorescent conjugated beads on the same system (Agilent, NovoCyte 3000) at the same time as cells, we could convert fluorescent intensity (FI) values to absolute numbers of binding molecules. The FI values were obtained with Novoexpress (Agilent) and analyzed in FlowJo.

J. Double emulsion encapsulates dextran preparation

The double emulsion droplets (DEDs) were generated using a flow-focusing microfluidic channel. The inner phase comprised 250 mM sucrose with 2 mg/ml FITC (fluorescein isothiocyanate). The oil phase comprised 7.5 mg/ml DOPC, 2.5 mg/ml DPPC, and 5 mg/ml cholesterol dissolved in oleic acid. A detailed droplet generation method and channel geometry can be found in our former study.[38] In brief, the inner and oil phases were sheared by an external phase (15% glycerol + 125 mM NaCl + 6% Pluronic F68), and droplets were pinched off. The DEDs were diluted in 1× PBS before sending to the flow cytometry.

1. Image data processing and analysis

High-speed images were recorded using a phantom high-speed camera (Vision Research, USA). The cell traveling distance was measured using ImageJ, an analysis software (https://imagej.nih.gov/ij/).

IV. DISCUSSION AND CONCLUSION

The antitumor efficacy of CAR T cells relies on the interactions between the receptors on engineered T cells and the ligands on the tumor cells. CAR is usually expressed by introducing tumor-specific gene sequences against tumor antigens such as anti-CD19 into the nucleus of T cells. The density of CAR molecules on the membrane of CAR T cells influences their heterogeneity, thereby affecting their functionalities and antitumor efficacies.[39,40] More specifically, CAR^High T cells are associated with excessive cytokine release, whereas CAR^Low T cells are not equipped with effective ligands that interact with tumor cells. The traditional non-viral approach used to introduce CAR genes is bulk electroporation, which operates on the principle of an electrical field opening and expanding nanopores on the cell membrane.[21] However, bulk electroporation applies an undesired strong electrical field to initiate membrane pores, damaging cell viability.[41] We recognize the transfection efficiency of the electroporator system used in this study can be further increased by exploring different input programs or optimizing T-cell activation and expansion conditions.[42] However, we believe an improvement in T-cell growth conditions will also improve the transfection efficiency of the AESOP platform. To date, there are few reported bulk electroporation platforms capable of controlling CAR expressions on the surface of T-cell membranes to produce homogeneous CAR T cells, particularly in human primary T cells. Moreover, most platforms do not prove uniform delivery through the characterization of CAR surface density.

In previous studies, we have shown that AESOP permeabilizes the cell membrane and controls cellular dosage uptake efficiently,

precisely, and in high throughput. AESOP consists of a two-step membrane disruption strategy: mechanical shear pore initialization and electrical field pore modulation. First, AESOP employs LCAT's bubble oscillation and microstreaming vortices to apply gentle, tunable, and uniform mechanical shear on cells near oscillating air-liquid interfaces to uniformly create nanopores on their membranes. Second, these nanopores are enlarged upon uniform exposure of the cells to gentle, low-strength electric fields. After nanopore creation and expansion on cell membranes, acoustic microstreaming generates chaotic mixing to ensure that the cargo can be uniformly and efficiently delivered into the cells. Cells continuously mix with cargoes in acoustic microstreaming vortices, resulting in a uniform cellular uptake across the cell population.

To adopt CAR T-cell therapy in clinical settings, it is critical to satisfy the requirements for high-throughput cell processing.[43] On average, many CAR T cells, ranging from millions to billions, are sufficient to eradicate tumors for successful treatment outcomes and patient survival. In this study, we modified our AESOP design to further increase the cell-processing density and speed from the previously reported 10^6 cells per minute per chip to 3×10^6 cells per minute per chip. Specifically, seven parallel microchannels with one shared inlet and one outlet intensified the bulk fluid containing T cells and mRNA cargoes to facilitate sample pumping/processing. Increasing the channel height from 40 to $60\,\mu m$ further enhanced throughput from 1.5×10^6 cells per minute for each chip to 3×10^6 cells per minute for each chip. We are exploring the development of an even higher throughput, $10–100 \times 10^6$ cell capacity system, using larger or multiple piezoelectric transducers and a larger configuration of gold-patterned electrodes to accommodate higher doses of CAR T cells needed in the clinic. Another potential adjustment to improve throughput is increasing the chip's width and height. Alternatively, our platform supports batch processing by leveraging its self-pumping and cell trapping capabilities.

Our group previously demonstrated that AESOP enabled the delivery of 6.1 kbp eGFP and 9.3 kbp CRISPR-Cas9 plasmids with high efficiency and viability. While the study provided a proof of concept that plasmid encoding CAR genes, with a size of approximately 9 kbp[33] delivered into T cells using AESOP is possible, delivery using plasmid for CAR T-cell generation has several limitations: Plasmids need to enter the cell nucleus, and then become transcribed into mRNA. Once mRNA is formed, the mRNA molecule is released into the cytoplasm and translated into a protein. Consequently, plasmid delivery is slower than direct mRNA delivery and poses delayed manufacturing challenges. More importantly, CD19-directed CAR T cells target both cancerous and normal B cells, and the elimination of all CD19-positive cells potentially results in B-cell aplasia.[44] Since plasmid-delivered CAR T cells exhibit permanent CAR expression, integrating the new genome into the host nucleus presents several safety concerns owing to the insertion of foreign genetic materials and immunogenicity. Furthermore, the size of the plasmid (5–9 kbp)[33] is much larger than that of mRNA (300–500 base pairs)[45] and is more challenging to deliver. In contrast to plasmids, mRNA allows for the transient expression of CAR as it is translated without genomic integration and has the potential to cause fewer on-target, off-tumor effects. Most synthetic mRNA molecules can be designed quickly and mass-produced cost-effectively. Additionally, the amount of mRNA

delivered to T cells affects the level of CAR expression in T cells, indicating that mRNA-based CAR expressions may offer a means to modulate the side effects associated with CAR T-cell therapy, such as cytokine release syndrome. In this study, we have shown that AESOP precisely controls the amount of intracellular dextran expression under different input dextran doses from 0.5 to $1.5\,\mu g$ while bulk electroporation consistently generates the same intracellular dextran expression under different input dextran doses from 0.5 to $1.5\,\mu g$. This highlights the ability of AESOP to control the amount of protein expression and generate homogeneous cells. We then further expanded the study to develop CAR T cells that expressed anti-CD19 using AESOP, and our results demonstrate a dosage-controlled anti-CD19 expression (greater than 65%) from CAR^{High}, CAR^{Medium} to CAR^{Low}. This lends itself to more precise cell engineering applications, and, to the best of our knowledge, no other studies have demonstrated the ability to titrate the CAR expression. Furthermore, we used %CV and an antibody-binding capacity assay to indicate the relative dispersion of the amount of mRNA delivered to the cell population, and our study showed that %CV <60 can be achieved by AESOP. Compared to the commercial Lonza electroporation platform, AESOP also demonstrated a significantly higher cell viability and transfection efficiency. These are particularly important for controlling uniform CAR expressions while reducing the cost associated with CAR T-cell generation.

In summary, AESOP provides a well-controlled process with a minimal benchtop space requirement capable of generating uniform CAR T cells for clinical applications. Moreover, our platform can be used to study the effect of CAR density on T-cell functionality and clinical responses in cancer treatment. Future work will involve testing the co-culture of CAR T cells with cancer cells and examining cytotoxicity, cell exhaustion, and cytokine release in a more physiological anticancer environment. AESOP can also be used to engineer a variety of cells more precisely, such as stem cells, dendritic cells, and macrophages. Finally, the comprehension of fluid mechanics and electroporation offers an important tool for identifying new physical approaches for controlled, uniform protein expressions that can be used to develop new cell therapies.

SUPPLEMENTARY MATERIAL

See the supplementary material for additional figures and notes on shear calculations, plasmids, and flow cytometry.

ACKNOWLEDGMENTS

AUTHOR DECLARATIONS
Conflict of Interest

The authors declare the following competing financial interests: The Regents of the University of California have filed patents related to the work described in the manuscript that A.P.L. and

Y.-H.C. are inventors. A.P.L. is a co-founder and has a financial interest in Cellecho Biotechnologies, which is commercializing the AESOP technology. The Regents of the University of California have financial interests in Cellecho Biotechnologies. This work has been previously submitted to a preprint server: Chen, Y.-H., Jiang, R., Lee, A.P., "Titering of Chimeric Antigen Receptors on CAR T Cells enabled by a Microfluidic-based Dosage-Controlled Intracellular mRNA Delivery Platform," bioRxiv, March 15, 2023, 2023.03.14.532624, ver. 1, https://www.biorxiv.org/content/10.1101/2023.03.14.532624v1.

Author Contributions

Y.-H.C. and M.M. have contributed equally to this work and designated as co-first authors.

Yu-Hsi Chen: Conceptualization (lead); Data curation (lead); Formal analysis (lead); Investigation (lead); Methodology (lead); Validation (lead); Visualization (lead); Writing – original draft (lead); Writing – review & editing (lead). **Mahnoor Mirza:** Conceptualization (equal); Data curation (equal); Formal analysis (equal); Investigation (equal); Methodology (equal); Validation (equal); Visualization (equal); Writing – original draft (lead); Writing – review & editing (lead). **Ruoyu Jiang:** Data curation (supporting); Methodology (supporting). **Abraham P. Lee:** Conceptualization (equal); Formal analysis (equal); Funding acquisition (lead); Investigation (supporting); Methodology (supporting); Project administration (equal); Resources (lead); Supervision (lead); Writing – review & editing (supporting).

DATA AVAILABILITY

The data that support the findings of this study are available within the article and its supplementary material.

REFERENCES

[1]J. H. Park, I. Rivière, M. Gonen, X. Wang, B. Sénéchal, K. J. Curran, C. Sauter, Y. Wang, B. Santomasso, E. Mead, M. Roshal, P. Maslak, M. Davila, R. J. Brentjens, and M. Sadelain, N. Engl. J. Med. **378**, 449 (2018).

[2]S. L. Maude, T. W. Laetsch, J. Buechner, S. Rives, M. Boyer, H. Bittencourt, P. Bader, M. R. Verneris, H. E. Stefanski, G. D. Myers, M. Qayed, B. De Moerloose, H. Hiramatsu, K. Schlis, K. L. Davis, P. L. Martin, E. R. Nemecek, G. A. Yanik, C. Peters, A. Baruchel, N. Boissel, F. Mechinaud, A. Balduzzi, J. Krueger, C. H. June, B. L. Levine, P. Wood, T. Taran, M. Leung, K. T. Mueller, Y. Zhang, K. Sen, D. Lebwohl, M. A. Pulsipher, and S. A. Grupp, N. Engl. J. Med. **378**, 439 (2018).

[3]A. Yip and R. M. Webster, Nat. Rev. Drug Discov. **17**, 161 (2018).

[4]S. S. Neelapu, F. L. Locke, N. L. Bartlett, L. J. Lekakis, D. B. Miklos, C. A. Jacobsen, I. Braunschweig, O. O. Oluwole, T. Siddiqi, Y. Lin, J. M. Timmerman, P. J. Stiff, J. W. Friedberg, I. W. Flinn, A. Goy, B. T. Hill, M. R. Smith, A. Deol, U. Farooq, P. McSweeney, J. Munoz, I. Avivi, J. E. Castro, J. R. Westin, J. C. Chavez, A. Ghobadi, K. V. Komanduri, R. Levy, E. D. Jacobsen, T. E. Witzig, P. Reagan, A. Bot, J. Rossi, L. Navale, Y. Jiang, J. Aycock, M. Elias, D. Chang, J. Wiezorek, and W. Y. Go, N. Engl. J. Med. **377**, 26 (2017).

[5]R. Voelker, JAMA **324**, 832 (2020).

[6]G. Ferrer, D. Álvarez-Errico, and M. Esteller, J. Natl. Cancer Inst. **114**, 930 (2022).

[7]C. L. Bonifant, H. J. Jackson, R. J. Brentjens, and K. J. Curran, Mol. Ther. Oncolytics **3**, 16011 (2016).

[8]J.-Y. Ho, L. Wang, Y. Liu, M. Ba, J. Yang, X. Zhang, D. Chen, P. Lu, and J. Li, Mol. Ther. Methods Clin. Dev. **21**, 237 (2021).

[9]P. Rodriguez-Marquez, M. E. Calleja-Cervantes, G. Serrano, A. Oliver-Caldes, M. L. Palacios-Berraquero, A. Martin-Mallo, C. Calviño, M. Español-Rego, C. Ceballos, T. Lozano, P. San Martin-Uriz, A. Vilas-Zornoza, S. Rodriguez-Diaz, R. Martinez-Turrillas, P. Jauregui, D. Alignani, M. C. Viguria, M. Redondo, M. Pascal, B. Martin-Antonio, M. Juan, A. Urbano-Ispizua, P. Rodriguez-Otero, A. Alfonso-Pierola, B. Paiva, J. J. Lasarte, S. Inoges, A. Lopez-Diaz de Cerio, J. San-Miguel, C. Fernandez de Larrea, M. Hernaez, J. R. Rodriguez-Madoz, and F. Prosper, Sci. Adv. **8**, eabo0514 (2022).

[10]X. Wang and I. Rivière, Mol. Ther. Oncolytics **3**, 16015 (2016).

[11]S. Hacein-Bey-Abina, A. Garrigue, G. P. Wang, J. Soulier, A. Lim, E. Morillon, E. Clappier, L. Caccavelli, E. Delabesse, K. Beldjord, V. Asnafi, E. MacIntyre, L. Dal Cortivo, I. Radford, N. Brousse, F. Sigaux, D. Moshous, J. Hauer, A. Borkhardt, B. H. Belohradsky, U. Wintergerst, M. C. Velez, L. Leiva, R. Sorensen, N. Wulffraat, S. Blanche, F. D. Bushman, A. Fischer, and M. Cavazzana-Calvo, J. Clin. Invest. **118**, 3132 (2008).

[12]K. Lundstrom, Diseases **6**, 42 (2018).

[13]J. Eyquem, J. Mansilla-Soto, T. Giavridis, S. J. C. van der Stegen, M. Hamieh, K. M. Cunanan, A. Odak, M. Gönen, and M. Sadelain, Nature **543**, 113 (2017).

[14]H. Singh, H. Huls, P. Kebriaei, and L. J. N. Cooper, Immunol. Rev. **257**, 181 (2014).

[15]P. J. Canatella, J. F. Karr, J. A. Petros, and M. R. Prausnitz, Biophys. J. **80**, 755 (2001).

[16]V. Lukjanov, I. Koutná, and P. Šimara, J. Immunol. Res. **2021**, 1–98.

[17]T. DiTommaso, J. M. Cole, L. Cassereau, J. A. Buggé, J. L. S. Hanson, D. T. Bridgen, B. D. Stokes, S. M. Loughhead, B. A. Beutel, J. B. Gilbert, K. Nussbaum, A. Sorrentino, J. Toggweiler, T. Schmidt, G. Gyuelveszi, H. Bernstein, and A. Sharei, Proc. Natl. Acad. Sci. U.S.A. **115**, E10907 (2018).

[18]Y. Cao, E. Ma, S. Cestellos-Blanco, B. Zhang, R. Qiu, Y. Su, J. A. Doudna, and P. Yang, Proc. Natl. Acad. Sci. U.S.A. **116**, 7899 (2019).

[19]C. A. Lissandrello, J. A. Santos, P. Hsi, M. Welch, V. L. Mott, E. S. Kim, J. Chesin, N. J. Haroutunian, A. G. Stoddard, A. Czarnecki, J. R. Coppeta, D. K. Freeman, D. A. Flusberg, J. L. Balestrini, and V. Tandon, Sci. Rep. **10**, 18045 (2020).

[20]J. A. Jarrell, A. A. Twite, K. H. W. J. Lau, M. N. Kashani, A. A. Lievano, J. Acevedo, C. Priest, J. Nieva, D. Gottlieb, and R. S. Pawell, Sci. Rep. **9**, 3214 (2019).

[21]A. Liu, M. Islam, N. Stone, V. Varadarajan, J. Jeong, S. Bowie, P. Qiu, E. K. Waller, A. Alexeev, and T. Sulchek, Mater. Today **21**(7), 703–712 (2018).

[22]J. Yen, M. Fiorino, Y. Liu, S. Paula, S. Clarkson, L. Quinn, W. R. Tschantz, H. Klock, N. Guo, C. Russ, V. W. C. Yu, C. Mickanin, S. C. Stevenson, C. Lee, and Y. Yang, Sci. Rep. **8**(1), 16304 (2018).

[23]X. Xie, A. M. Xu, S. Leal-Ortiz, Y. Cao, C. C. Garner, and N. A. Melosh, ACS Nano **7**, 4351–4358 (2013).

[24]P. Chakrabarty, P. Gupta, K. Illath, S. Kar, M. Nagai, F.-G. Tseng, and T. S. Santra, Mater. Today Bio. **13**, 100193 (2022).

[25]M. Aghaamoo, Y.-H. Chen, X. Li, N. Garg, R. Jiang, J. T.-H. Yun, and A. P. Lee, Adv. Sci. **9**, 2102021 (2022).

[26]N. Pardi, M. J. Hogan, F. W. Porter, and D. Weissman, Nat. Rev. Drug Discov. **17**, 261 (2018).

[27]T. Soundara Rajan, A. Gugliandolo, P. Bramanti, and E. Mazzon, Int. J. Mol. Sci. **21**, 6514 (2020).

[28]R. S. Riley, C. H. June, R. Langer, and M. J. Mitchell, Nat. Rev. Drug Discov. **18**, 175 (2019).

[29]M. V. Maus, A. R. Haas, G. L. Beatty, S. M. Albelda, B. L. Levine, X. Liu, Y. Zhao, M. Kalos, and C. H. T. June, Cancer Immunol. Res. **1**, 26–31 (2013).

[30]A. Moretti, M. Ponzo, C. A. Nicolette, I. Y. Tcherepanova, A. Biondi, and C. F. Magnani, Front. Immunol. **13**, 867013 (2022).

[31]G. Tavernier, O. Andries, J. Demeester, N. N. Sanders, S. C. De Smedt, and J. Rejman, J. Controlled Release **150**(3), 238–247 (2011).

[32]K. Xiao, Y. Lai, W. Yuan, S. Li, X. Liu, Z. Xiao, and H. Xiao, Interdiscip. Med. **2**(1), e20230036 (2024).

[33]D. Bloemberg, T. Nguyen, S. MacLean, A. Zafer, C. Gadoury, K. Gurnani, A. Chattopadhyay, J. Ash, J. Lippens, D. Harcus, M. Pagé, A. Fortin, R. A. Pon, R. Gilbert, A. Marcil, R. D. Weeratna, and S. McComb, Mol. Ther. Methods Clin. Dev. **16**, 238 (2020).

[34]X. Liu, Y. Wang, H. Lu, J. Li, X. Yan, M. Xiao, J. Hao, A. Alekseev, H. Khong, T. Chen, R. Huang, J. Wu, Q. Zhao, Q. Wu, S. Xu, X. Wang, W. Jin, S. Yu, Y. Wang, L. Wei, A. Wang, B. Zhong, L. Ni, X. Liu, R. Nurieva, L. Ye, Q. Tian, X.-W. Bian, and C. Dong, Nature **567**, 525 (2019).

[35]A. Nock, Chromosoma **83**, 209 (1981).

[36]A. R. Tovar and A. P. Lee, "Lateral cavity acoustic transducer," Lab Chip **9**, 41–43 (2009).

[37]Y. Liu, A. Beyer, and R. Aebersold, Cell **165**, 535 (2016).

[38]J.-Y. Chen, S. Agrawal, H.-P. Yi, D. Vallejo, A. Agrawal, and A. P. Lee, Adv. Healthcare Mater. **12**, 2203163 (2023).

[39]R. G. Majzner, S. P. Rietberg, E. Sotillo, R. Dong, V. T. Vachharajani, L. Labanieh, J. H. Myklebust, M. Kadapakkam, E. W. Weber, A. M. Tousley, R. M. Richards, S. Heitzeneder, S. M. Nguyen, V. Wiebking, J. Theruvath, R. C. Lynn, P. Xu, A. R. Dunn, R. D. Vale, and C. L. Mackall, Cancer Discov. **10**, 702 (2020).

[40]F. L. Locke, J. M. Rossi, S. S. Neelapu, C. A. Jacobson, D. B. Miklos, A. Ghobadi, O. O. Oluwole, P. M. Reagan, L. J. Lekakis, Y. Lin, M. Sherman, M. Better, W. Y. Go, J. S. Wiezorek, A. Xue, and A. Bot, Blood Adv. **4**, 4898 (2020).

[41]T. Kotnik, G. Pucihar, and D. Miklavčič, J. Membrane Biol. **236**, 3 (2010).

[42]N. von Auw, R. Serfling, R. Kitte, N. Hilger, C. Zhang, C. Gebhardt, A. Duenkel, P. Franz, U. Koehl, S. Fricke, and U. S. Tretbar, Sci. Rep. **13**(1), 18160 (2023).

[43]J. Hartmann, M. Schüßler-Lenz, A. Bondanza, and C. J. Buchholz, EMBO Mol. Med. **9**, 1183 (2017).

[44]Q. Deng, G. Han, N. Puebla-Osorio, M. C. J. Ma, P. Strati, B. Chasen, E. Dai, M. Dang, N. Jain, H. Yang, Y. Wang, S. Zhang, R. Wang, R. Chen, J. Showell, S. Ghosh, S. Patchva, Q. Zhang, R. Sun, F. Hagemeister, L. Fayad, F. Samaniego, H. C. Lee, L. J. Nastoupil, N. Fowler, R. Eric Davis, J. Westin, S. S. Neelapu, L. Wang, and M. R. Green, Nat. Med. **26**, 1878 (2020).

[45]N. N. Parayath, S. B. Stephan, A. L. Koehne, P. S. Nelson, and M. T. Stephan, Nat. Commun. **11**, 6080 (2020).